Inorganic Chemistry

Article

pubs.acs.org/IC

Copper(I) Nitro Complex with an Anionic $[HB(3,5\text{-}Me_2Pz)_3]^-$ Ligand: A Synthetic Model for the Copper Nitrite Reductase Active Site

Sodio C. N. Hsu,*[,†] Yu-Lun Chang,[†,‡] Wan-Jung Chuang,[†] Hsing-Yin Chen,*[,†] I-Jung Lin,[†] Michael Y. Chiang,[‡] Chai-Lin Kao,[†] and Hsuan-Ying Chen[†]

[†]Department of Medicinal and Applied Chemistry, Kaohsiung Medical University, Kaohsiung 807, Taiwan

[‡]Department of Chemistry, National Sun Yat-Sen University, Kaohsiung 804, Taiwan

Supporting Information

ABSTRACT: The new copper(I) nitro complex $[(Ph_3P)_2N][Cu(HB(3,5\text{-}Me_2Pz)_3)(NO_2)]$ (**2**), containing the anionic hydrotris(3,5-dimethylpyrazolyl)borate ligand, was synthesized, and its structural features were probed using X-ray crystallography. Complex **2** was found to cocrystallize with a water molecule, and X-ray crystallographic analysis showed that the resulting molecule had the structure $[(Ph_3P)_2N][Cu(HB(3,5\text{-}Me_2Pz)_3)(NO_2)]\cdot H_2O$ (**3**), containing a water hydrogen bonded to an oxygen of the nitrite moiety. This complex represents the first example in the solid state of an analogue of the nitrous acid intermediate ($CuNO_2H$). A comparison of the nitrite reduction reactivity of the electron-rich ligand containing the $CuNO_2$ complex **2** with that of the known neutral ligand containing the $CuNO_2$ complex $[Cu(HC(3,5\text{-}Me_2Pz)_3)(NO_2)]$ (**1**) shows that reactivity is significantly influenced by the electron density around the copper and nitrite centers. The detailed mechanisms of nitrite reduction reactions of **1** and **2** with acetic acid were explored by using density functional theory calculations. Overall, the results of this effort show that synthetic models, based on neutral $HC(3,5\text{-}Me_2Pz)_3$ and anionic $[HB(3,5\text{-}Me_2Pz)_3]^-$ ligands, mimic the electronic influence of $(His)_3$ ligands in the environment of the type II copper center of copper nitrite reductases (Cu-NIRs).

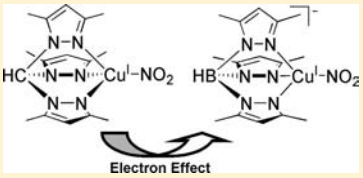

INTRODUCTION

The active sites of copper-containing nitrite reductases (Cu-NIRs), which transform NO_2^- to NO, contain a type I electron-transfer center that is coupled via a His-Cys bridge to a type II catalytic center.[1−10] The results of numerous spectroscopic and crystallographic studies have led to proposed mechanisms (Scheme 1) for catalysis by the Cu-NIRs,[11−22] which involve the formation of copper(I) nitro or nitrito core species by either the reduction of oxidized Cu-NIRs followed by nitrite anion binding or the binding of nitrite to oxidized Cu-NIRs first followed by reduction. In the next step of the catalytic pathway, the copper(I) nitro or nitrito species is protonated by an adjacent aspartate residue (Asp98), forming a copper nitrosyl intermediate. Finally, NO is displaced from the copper by water, regenerating the active enzyme.

Because of the proposed key role they play in catalysis by the Cu-NIRs, copper(I) nitro or nitrito complexes have been important targets of structural and chemical studies. However, the preparation of these substances has remained challenging, and only a few copper(I) nitro complexes have been characterized thus far by using single-crystal X-ray methods.[23−28] In one effort, Tolman and co-workers synthesized the first functional, mononuclear biomimetic model of the copper centers in Cu-NIRs. The nitro-binding copper(I) complex $[(^{i}Pr\text{-}TACN)Cu(NO_2)]$ (^{i}Pr-TACN = 1,4,7-triisopropyl-1,4,7-triazacyclononane) prepared in this study was observed to evolve nitric oxide gas through reaction with 2 equiv of acetic acid.[23] The results of related investigations,[29] aimed at examining the protonation reaction by using spectroscopic titration of the copper(I) nitro complex reduction process, have led to the proposal that a nitrous acid intermediate ($CuNO_2H$) exists in the process. Observations made in recent studies[28] show that sterically hindered tris(1-pyrazolyl)methane (TPM) and tris(4-imidazolyl)carbinol (TIC) tridentate ligands in model copper(I) nitro complexes exert steric and weak electronic effects. Independently, we and others have described rare copper(I) nitrito phosphine complexes, which also react to form nitric oxide gas when treated with acetic acid under anaerobic conditions.[30,31] Therefore, these complexes serve as functional but not structural models for Cu-NIRs. Recently, the first example of a monomeric copper(I) nitrito complex, containing two bidentate nitrogen ligands, was described,[32] but its catalytic activity was not evaluated.

Another important bioinorganic mimicking ligand, hydrotris(pyrazolyl)borate anion (^{RR}Tp), has been used to construct a copper(II) nitrito complex ($^{RR}TpCuNO_2$)[33−35] and structurally models of the copper nitrosyl intermediate ($^{RR}TpCuNO$).[36−39] Hydrotris(triazolyl)borate, a ^{RR}Tp analogue, has recently been used as a ligand in $CuNO_2$ complexes that have been probed as structural and functional models of Cu-NIRs.[40] Although a comparison of the properties of the copper(I) nitro of ^{RR}Tp with known copper(I) nitro complexes[28] containing TPM would provide important information about the ligand effects on the catalytic activities of Cu-NIRs, the ^{RR}Tp complex remains an unknown entity.[25]

Received: May 7, 2012
Published: August 20, 2012

   dx.doi.org/10.1021/ic300932a | *Inorg. Chem.* 2012, 51, 9297−9308

Scheme 1. Revised Mechanism for Catalysis by Cu-NIRs Based on the Results of Averill, Suzuki, and Hasnain[3,10,17,19]

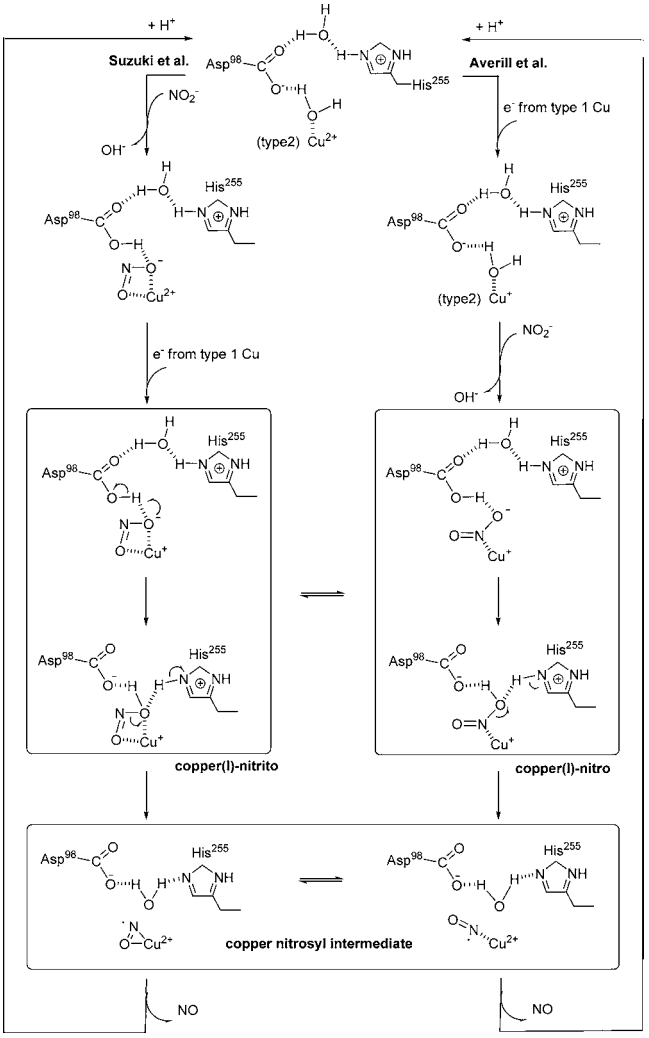

Below, we describe the results of an investigation that has led to the synthesis and structural characterization of a copper(I) nitro complex stabilized by the anionic tripodal scorpionate ligand hydrotris(3,5-dimethylpyrazolyl)borate ($[HB(3,5\text{-}Me_2Pz)_3]^-$) and a comparison of its properties with that of the known[28] copper(I) nitro complex stabilized by the neutral tris(3,5-dimethylpyrazolyl)methane $[HC(3,5\text{-}Me_2Pz)_3]$ ligand (Chart 1). Both complexes contain facially coordinating pyrazole groups that closely mimic the pyramidal array of histidine imidazoles that is present around copper in the type II active site of Cu-NIRs. Moreover, this study enabled an evaluation of how the electronic properties of the two differently charged ligands affect the electronic properties of the complexes. Significantly, as discussed below, the results of this effort demonstrate that the nitrite reductase reactivity of neutral and anionic copper(I) nitro complexes is significantly influenced by the electron density at the copper nitrite center.

Chart 1. Structures of the Tris(3,5-dimethylpyrazolyl)methane $HC(3,5\text{-}Me_2Pz)_3$ and Hydrotris(3,5-dimethylpyrazolyl)borate Anionic $[HB(3,5\text{-}Me_2Pz)_3]^-$ Ligands

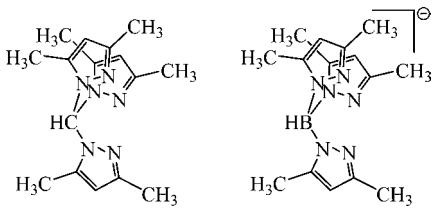

RESULTS AND DISCUSSION

Synthesis and Spectroscopic Characterization of Complexes 1 and 2. The neutral copper(I) nitro complex $[Cu(HC(3,5\text{-}Me_2Pz)_3)(NO_2)]$ (**1**) was prepared through the reaction of $[Cu(HC(3,5\text{-}Me_2Pz)_3)(NCMe)](BF_4)$[41] with $NaNO_2$ in methanol under N_2 and isolated as a pale-yellow solid (Scheme 2). An alternative method for the synthesis of complex **1** was reported in a publication[28] that appeared during the preparation of the current manuscript. Treatment of the dimeric complex $[HB(3,5\text{-}Me_2Pz)_3Cu]_2$[42] with an equimolar amount of $[(Ph_3P)_2N](NO_2)$ [$(Ph_3P)_2N$ = bis(triphenylphosphine)iminium] in tetrahydrofuran (THF) leads to formation of the novel mononuclear copper(I) nitro complex $[(Ph_3P)_2N][Cu(HB(3,5\text{-}Me_2Pz)_3)(NO_2)]$ (**2**), containing a negatively charged $[HB(3,5\text{-}Me_2Pz)_3]^-$ ligand. Crystallization of this substance from THF yields **2** as yellow crystals. When wet THF is employed in the crystallization process, an adventitious water molecule cocrystallizes with **2** to generate the pale-yellow complex $[(Ph_3P)_2N][Cu(HB(3,5\text{-}Me_2Pz)_3)(NO_2)]\cdot H_2O$ (**3**). For comparison purposes, an attempt was made to crystallize the copper(I) nitro complex **1** from wet THF. However, in this case, a crystalline complex containing water was not produced.

Scheme 2. Method for the Synthesis of Copper(I) Nitro Complexes 1 and 2

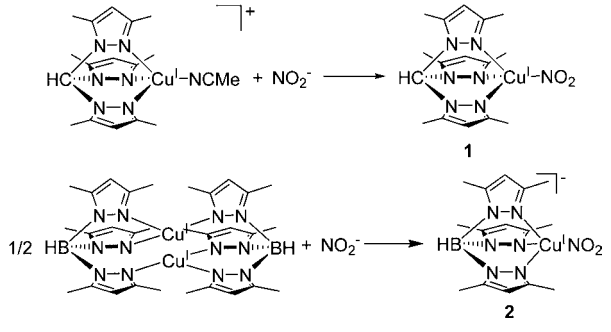

The structures of copper(I) nitro complexes **1** and **2** were initially assigned using ^1H NMR spectroscopy and elemental analysis. The electrospray ionization mass spectrometry (ESI-MS) data of **1** and **2** contain characteristic molecular ion peaks and corresponding fragment ion peaks corresponding to the loss of coordinated NO_2. Also, UV–vis spectra of complexes **1** and **2** also contain diagnostic metal-to-ligand charge-transfer (MLCT) bands at 293 and 336 nm, respectively (Figure 1). The difference seen in the positions of the MLCT absorption bands could be a consequence of the dissimilar electronic structures of **1** and **2**. The IR spectra of **1** and **2**, measured using KBr pellets, contain NO_2 stretching bands for the anion **2** at 1302 and 1267 cm^{-1}, which are shifted to lower frequencies than those (1312 and 1285 cm^{-1}) for the same stretching modes in the neutral complex **1**. This observation suggests that the neutral $[Cu(HB(3,5\text{-}Me_2Pz)_3)]$ moiety present in **2** causes a stronger $Cu^I \rightarrow NO_2^-$ π-back-bonding interaction than does

dx.doi.org/10.1021/ic300932a | Inorg. Chem. 2012, 51, 9297–9308

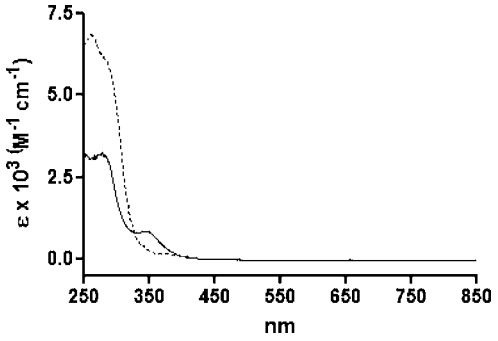

Figure 1. Absorption spectra of **1** (dashed line) and **2** (solid line) in CH_2Cl_2 at room temperature.

the positive $[Cu(HC(3,5\text{-}Me_2Pz)_3)]$ moiety in **1**. The same trend has been observed earlier in studies of copper(I) acetonitrile and carbonyl complexes containing similar methane and borate ligands.[43]

To explore the electronic effects exerted by the negatively charged borate ligand versus the corresponding neutral methane ligand, cyclic voltammetric measurements with **2** (Figure S4 in the Supporting Information) in CH_2Cl_2 containing 0.1 M $[n\text{-}Bu_4N](PF_6)$ were made and compared with those of the known complex **1**. Complex **1** exhibits a quasi-reversible one-electron peak ($E_{1/2}$ = 0.25 V; E_{pa} = 0.39 V), assigned to the Cu^I/Cu^{II} redox process.[28] In contrast, the cyclic voltamagram of **2** contains an irreversible band corresponding to an E_{pa} value of 0.08 V, which is significantly lower than that of **1**. The results of the electrochemistry study show that oxidation of complex **2** with the negative $HB(3,5\text{-}Me_2Pz)_3^-$ ligand is more favorable than that of the neutral $HC(3,5\text{-}Me2Pz)_3$ ligand containing complex **1**. This finding indicates that the redox potentials of copper(I) nitro complexes are governed by the electronic nature of the tridentate ligands [negative $HB(3,5\text{-}Me_2Pz)_3^-$ ligand versus neutral $HC(3,5\text{-}Me2Pz)_3$ ligand].

Structural Studies of Copper(I) Nitro Complexes 2 and 3. The ORTEP representations of the X-ray crystallographic structures of complexes **2** and **3** are shown in Figures 2 and 3, respectively. Inspection of the plots show that *N*-nitro coordination to the copper(I) center exists in each structure.

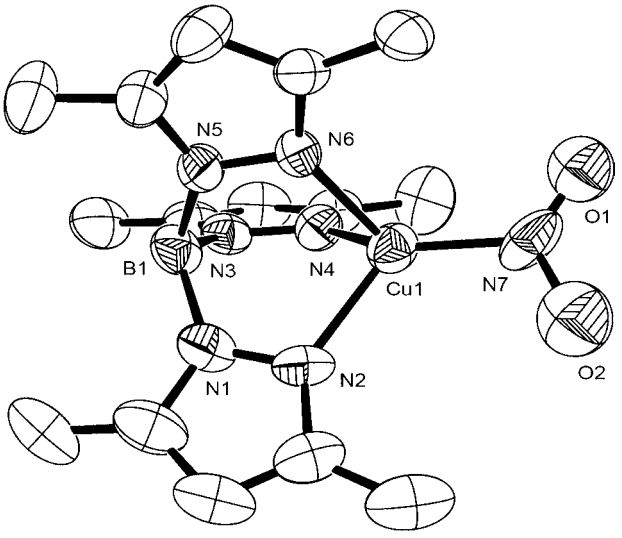

Figure 2. ORTEP representation of an anion of the X-ray structure of **2** (50% ellipsoids; hydrogen atoms not shown for clarity).

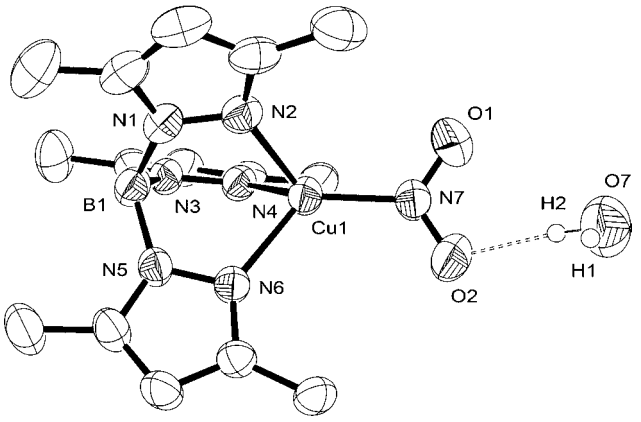

Figure 3. ORTEP representation of an anion of the X-ray structure of **3** (50% ellipsoids; some hydrogen atoms not shown for clarity).

Selected bond lengths and angles of the complexes are listed in Table 1 along with those of known complex **1** for comparison.[28] The coordination geometry around the copper atom of **2** and **3**, both of which contain chelated facial anionic tridentate $[HB(3,5\text{-}Me_2Pz)_3]^-$ ligands, is best described as a distorted tetrahedron. This feature is similar to that of **1**, which contains a chelated facial neutral $HC(3,5\text{-}Me_2Pz)_3$ auxiliary ligand. It is noteworthy that a moderate hydrogen-bond interaction, associated with an $O(w)\text{–}O(NO_2)$ distance of 2.898 Å,[44] occurs between one of the oxygen atoms of the copper(I) nitro unit and the cocrystallized water molecule in **3**. The presence of this hydrogen-bonded (H-bonded) water molecule suggests that the borate complex **2** might display a higher reactivity toward protic solvents or acids. Indeed, complex **2** is observed to decompose in a methanol solution, while **1** is moderately stable under similar conditions. Recently, Kujime et al. was able to detect the nitrous acid intermediate ($CuNO_2H$) in nitrite reduction brought about by the rapid mixing of $[(^i\text{Pr-TACN})Cu(NO_2)]$ with trifluoroacetic acid at low temperature in a stopped-flow apparatus.[29] Consequently, complex **3**, with hydrogen-bond interaction between a water molecule and an oxygen atom of the copper(I) nitro unit, represents the first solid-state example of an analogue of the nitrous acid intermediate ($CuNO_2H$).

The structures of the copper(I) nitro complexes are governed by the nature of their tridentate neutral $HC(3,5\text{-}Me_2Pz)_3$ and negatively charged $[HB(3,5\text{-}Me_2Pz)_3]^-$ ligands. The intraligand $N_L\text{–}Cu\text{–}N_L$ angles are restrained by the chelate rings to 87.1° for **1**, 90.0° for **2**, and 90.3° for **3**, and the averages of the angles from nitrogen atoms of the nitrite donors to the pyrazolyl nitrogen atoms are 127.20° for **1**, 125.22° for **2**, and 124.98° for **3**. The nitrite O–N–O angle [122.8(3)°] of **3** is larger than the corresponding value for **1** [117.4(5)°], **2** [116.7(7)°], and a free nitrite anion [114.9(5)°],[45] possibly as a result of hydrogen-bond perturbation caused by the cocrystallized water molecule in **3**. The $Cu\text{–}N_L$ distances in the tridentate ligands of **1**–**3**, ranging from of 2.046 to 2.113 Å, are similar. Importantly, the $Cu\text{–}N_{nitro}$ distance in **2** [1.927(5) Å] is relatively larger than that in **1** [1.883(6) Å], indicating the role played by the charge of the borate versus the methane ligands containing identical pyrazolyl substituents. Thus, the cationic $[Cu(HC(3,5\text{-}Me_2Pz)_3)]^+$ moiety interacts more

dx.doi.org/10.1021/ic300932a | Inorg. Chem. 2012, 51, 9297–9308

Table 1. Selected Bond Lengths (Å) and Angles (deg) for 2 and 3 and Other Relevant Copper(I) Nitro Complexes

	$Cu-N_{nitro}$	N−O	$Cu-N_L$	O−N−O	N_L-Cu-N_{nitro}	N_L-Cu-N_L	ref
1	1.883(6)	1.176(7)	2.051(3)	117.4(5)	126.7(1)	86.2(2)	28
		1.278(7)	2.051(3)		126.7(1)	87.6(1)	
			2.124(5)		128.4(2)	87.6(2)	
2	1.927(5)	1.212(9)	2.070(3)	116.7(7)	121.07(19)	89.17(16)	this work
		1.290(12)	2.078(5)	116.8(8)[a]	126.38(19)	90.19(14)	
		1.161(10)[a]	2.103(4)		128.2(2)	90.51(17)	
		1.332(13)[a]					
3	1.903(3)	1.224(4)	2.046(4)	122.8(3)	121.14(11)	88.82(9)	this work
		1.224(4)	2.089(3)		123.75(10)	90.45(10)	
			2.113(2)		130.06(11)	91.65(9)	
$NaNO_2$		1.240(3)		114.9(5)			45

[a]Oxygen atoms in the copper-bound nitro were found to be disordered.

strongly with a nitrite anion than does the neutral [Cu(HB(3,5-$Me_2Pz)_3$)] moiety. The average of the two N−O distances (1.251 Å) of **2** is slightly larger than the corresponding values of **1** (1.227 Å) and a free nitrite [1.240(3) Å],[45] a finding that is consistent with the IR results. Again, these features may be a consequence of different electronic interactions of a nitrite ion with the positive $[Cu(HC(3,5\text{-}Me_2Pz)_3)]^+$ and neutral [Cu-(HB(3,5-$Me_2Pz)_3$)] moieties. A similar effect of the positive $[Cu(HC(3,5\text{-}Me_2Pz)_3)]^+$ and neutral [Cu(HB(3,5-$Me_2Pz)_3$)] moieties on π acceptors and σ donors has been discussed by Fujisawa et al.[43,46] The water-containing complex **3** has a smaller Cu−NO_2 distance [1.903(3) Å] than **2** [1.927(5) Å], showing that the hydrogen-bond interaction affects the properties of the copper(I) nitro bond.

Reactivity with Acid. In order to gain information about how the electronic effects govern the nitrite reductase activity of the copper(I) nitro complexes, containing neutral or anionic tridentate nitrogen-donor ligands, the reactivity of the anionic ligand containing complex **2** with proton sources was determined and compares with that of **1**, containing a neutral ligand. The results show that complex **2** is highly reactive toward acids, as shown by the immediate color change that occurs when the complex is subjected to acidic conditions. In contrast, **1** reacts more slowly with acid. In studies probing the reactivity toward oxygen, we observed that complex **2** is an extremely air-sensitive compound and that **1** is air- and moisture-stable in the solid state but air-sensitive in solution. These properties may also be a consequence of the different electronic nature of the $CuNO_2$ cores of **1** and **2**.

The results of this investigation show that the reaction of **1** with acetic acid is first-order with respect to **1**. The plots of pseudo-first-order rate constants for this process versus acetic acid concentration are curved rather than linear (Figure S5 in the Supporting Information), indicating the occurrence of a stepwise proton-transfer mechanism in agreement with the results of a previous study.[28] As mentioned above, in contrast to **1**, **2** is more reactive with acetic acid. The rate of reaction of **2** with acetic acid at 233 K was monitored by using UV−vis absorption spectroscopy. In the spectra, a decrease in the absorbance at 336 nm and a slight increase at 750 nm is observed as reaction occurs (Figure 4). The reaction of **2** with acid was found to be first-order in **2**, and the rate constant is linearly dependent on the concentration of acetic acid (Figure S6 in the Supporting Information). The difference in the rate expressions for reactions of **1** and **2** with acetic acid suggests that these processes have different rate-limiting steps associated with the electron-rich $CuNO_2$ moiety in **2**, which causes the

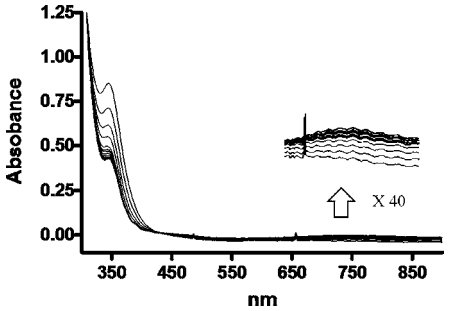

Figure 4. Spectral changes observed during the anaerobic reaction of **2** with acetic acid in CH_2Cl_2 at 233 K.

nitrite reduction step to be more rapid than it is in the reaction of complex **1**, containing the neutral ligand. The results of titration experiments using **1** and acetic acid show that 2 equiv of acetic acid is consumed in the reaction.[28] On the other hand, the same experiments with **2** clearly show that only 1 equiv of acetic acid is consumed in the reaction (see Figure S7 in the Supporting Information). This difference demonstrates that different mechanisms operate in the nitrite reduction reaction of **1** and **2**.

The products generated in reactions of **1** and **2** with both acetic and trifluoroacetic acid were isolated and shown using ESI-MS, elemental, and X-ray crystallographic analysis to be the respective complexes $[Cu(HC(3,5\text{-}Me_2Pz)_3)(CH_3COO)_2]$ (**4**), $[Cu(HB(3,5\text{-}Me_2Pz)_3)(CH_3COO)]$ (**5**), and $[Cu(HC(3,5\text{-}Me_2Pz)_3)(CF_3COO)_2]$ (**6**) (see below), in which an acetate (trifluoroacetate) anion is bound to the copper(II) ion.

The temperature dependencies of the rates of the nitrite reduction reactions of **1** and **2** were examined at four temperatures in the range of 223−273 K (Tables 2 and S1 in the Supporting Information). Analysis of the results using the typical Eyring approach (Figures S8 and S9 in the Supporting Information) gave the $\Delta H^{\ddagger}$ and $\Delta S^{\ddagger}$ values listed in Table 2. Comparisons of the activation parameters with those of the known copper(I) nitro complex $[Cu(Me_2bpa)(NO_2)]$[26] [Me_2bpa = bis(6-methyl-2-pyridylmethyl)amine] ($\Delta H^{\ddagger}$ = 25 ± 1 kJ mol^{-1} and $\Delta S^{\ddagger}$ = −51 ± 3 J K^{-1} mol^{-1}) reveals that reactions of **1** and **2** have significantly larger $\Delta H^{\ddagger}$ (32.96 ± 2.40 kJ mol^{-1} for **1**; 36.57 ± 2.25 kJ mol^{-1} for **2**) and more negative $\Delta S^{\ddagger}$ (−170.27 ± 9.68 J K^{-1} mol^{-1} for **1**; −115.40 ± 9.49 J K^{-1} mol^{-1} for **2**) values. Because a large negative $\Delta S^{\ddagger}$ value generally corresponds to reactions having rate-determining transition states involving the loss of translational degrees of freedom, the very large negative $\Delta S^{\ddagger}$ values for reactions of **1**

dx.doi.org/10.1021/ic300932a | Inorg. Chem. 2012, 51, 9297−9308

Table 2. Rate Constants for the Nitrite Reduction of Copper(I) Nitro Complexes (0.25 mM) with Excess Acetic Acid (25 mM)

	k_{obs} (s^{-1})	
temperature (K)	**1**	**2**
223		$(1.21 \pm 0.09) \times 10^{-2}$
233	$(2.80 \pm 1.30) \times 10^{-4}$	$(2.64 \pm 0.25) \times 10^{-2}$
243	$(5.00 \pm 1.00) \times 10^{-4}$	$(7.30 \pm 0.45) \times 10^{-2}$
253	$(9.33 \pm 1.15) \times 10^{-4}$	$(1.33 \pm 0.11) \times 10^{-1}$
273	$(3.90 \pm 0.60) \times 10^{-3}$	
	1	**2**
$\Delta H^{\ddagger}$ (kJ mol^{-1})	32.96 ± 2.40	36.57 ± 2.25
$\Delta S^{\ddagger}$ (J K^{-1} mol^{-1})	−170.27 ± 9.68	−115.40 ± 9.49

and **2** suggest that nearly complete associative proton transfer takes place in the transition state.

In order to further investigate the proton-transfer step in the nitrite reduction process, kinetic isotopic effect (KIE) experiments were carried out. The observed KIEs (k_H/k_D) for the protonation reactions of **1** and **2** were found to be ca. 1.73 and 0.93, respectively. Although little KIE data for reactions of the type have been accumulated thus far, studies have shown that the protonation reaction of the neutral [(^{i}Pr-TACN)Cu(NO_2)] complex has a k_H/k_D value of ca. 1.4 at 203 K.[29] The similarity of this KIE with that of the protonation reaction of **1** suggests theat they have similar rate-determining transition states. k_H/k_D = 0.93 for the reaction of **2** with acid, representing a small inverse KIE, suggests that the protonation step in the nitrite reduction reaction of this substance is not rate-determining and that further reaction of the deuterated intermediate derived from **2** is more stable relative to its protonated analogue. Importantly, these findings also indicate that protonation occurs through a late transition state involving hydrogen bonding between the acid and $CuNO_2$ core of **2**, prior to transfer of the proton to nitrite. The suggestion that this hydrogen-bond interaction leads to an inverse KIE is supported by the results of studies of the protonation reactions of metal hydride complexes.[47]

Structural Study of the Copper(II) Complex 6. As mentioned above, the reaction of complex **1** with trifluoroacetic acid produces **6**. Single crystals of **6** were grown by the slow diffusion of Et_2O into a mixture of **1** and trifluoroacetic acid. Inspection of the ORTEP plot of the crystallographic data (Figure 5) shows that the coordination sphere around the copper(II) ion in **6** has essentially a distorted square-pyramidal geometry, with the basal plane comprised of two nitrogen atoms, N2 and N4, from the tris(pyrazolyl)methane ligand and two oxygen atoms, O1 and O3, from two monodentate trifluoroacetate anions. The axial site in this geometry is occupied by the nitrogen N6 from the tris(pyrazolyl)methane ligand. This coordination geometry is supported by the observed structural parameter τ value of 0.21.[48] In contrast to related tris(pyrazolyl)methane- and tris(pyrazolyl)-boratecopper(II) complexes, the coordination geometry of **6** also contains a N_3O_2 coordination sphere, which has smaller τ value (<0.1).[33,49,50] These structural differences are presumably caused by unfavorable steric interactions between the trifluoromethyl and methyl groups on the tripodal scorpionate tris(pyrazolyl)methane ligand.

NO Generation. The fact that the anionic ligand containing complex **2** is more reactive toward protonation steps than its neutral analogue **1** suggests that the electronic effects could

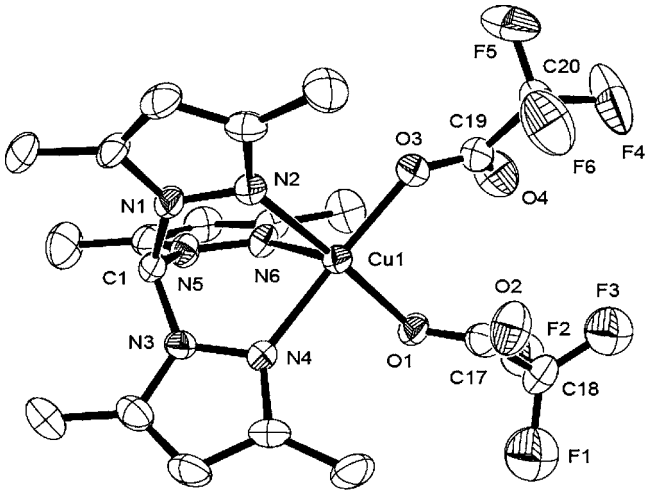

Figure 5. ORTEP representation of the X-ray structure of **6** (50% ellipsoids; hydrogen atoms not shown for clarity).

play an important role in nitrite reduction by the Cu-NIRs. Previously, the best models devised for Cu-NIR active sites were nitro-bonding copper(I) complexes containing neutral tridentate ligands, with the copper unit bearing ^{i}Pr-TACN, bis(6-methyl-2-pyridylmethyl)amine (Me_2bpa), or sterically hindered TIC and TPM ligands.[25,26,28] In contrast, **2** contains an electron-rich copper(I) nitro moiety, which might cause it to react efficiently with acid to yield nitric oxide in a process that mimics nitrite reduction by the Cu-NIRs.

To assess this issue, **2** and the known complex **1** were investigated for their NO-generating ability. The addition of 6 equiv of trifluoroacetic acid to independent oxygen-free CH_2Cl_2 solutions of **1** and **2** at room temperature promotes a color change from pale yellow to blue-green and stoichiometric evolution of NO gas (52.3 ± 3.72% for **1**; 83.3 ± 2.3% for **2**; Table 3), identified by using the known gas chromatography

Table 3. Yields of NO Generation from Reactions of 1 and 2 with Trifluoroacetic Acid in CH_2Cl_2

	yield (%)	
entry	**1**	**2**
1	55.1	81.2
2	53.8	85.8
3	48.1	82.8
average ± standard deviation	52.3 ± 3.72	83.3 ± 2.3

with a thermal conductivity detector (GC-TCD) method (Figure S10 in the Supporting Information).[25,26,30] Comparisons of the NO evolution results with those arising from studies of the known copper(I) nitro nitrogen ligand environment complexes [(^{i}Pr-TACN)Cu(NO_2)] (ca. 100%),[25] [Cu(Me_2bpa)(NO_2)] (ca. 95%),[26] and [(^{i}Pr-TIC)-Cu(NO_2)] [*i*Pr-TIC = tris(3,5-diisopropyl-1-pyrazoyl)-methane] (ca. 70%)[28] demonstrate that the copper(I) nitro complex **2** is also a good functional Cu-NIR model that produces NO in reaction with trifluoroacetic acid under anaerobic conditions. Importantly, no N_2O gas is produced, and the green-blue copper(II) products **6** and [Cu(HB(3,5-$Me_2Pz)_3$)(CF_3COO)] (**7**) (characterized by ESI-MS or crystallographic methods) are generated as products in the respective reactions of $CuNO_2$ complexes **1** and **2**.

dx.doi.org/10.1021/ic300932a | *Inorg. Chem.* 2012, 51, 9297−9308

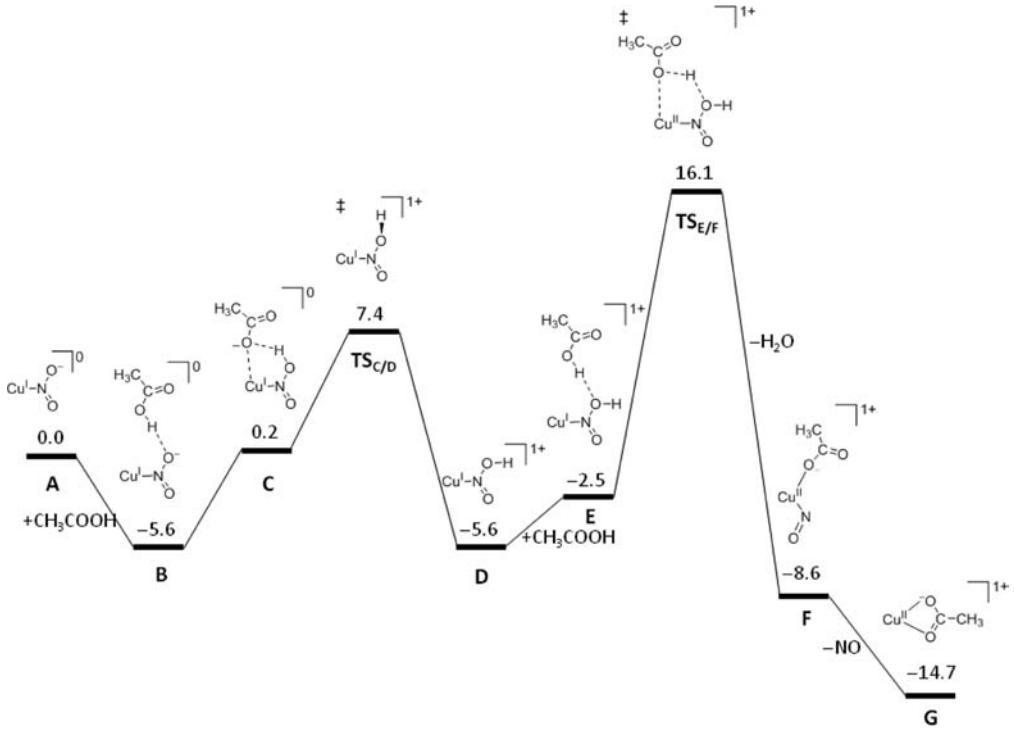

Figure 6. M06/6-31G* free-energy profile for nitrite reduction of **1**.

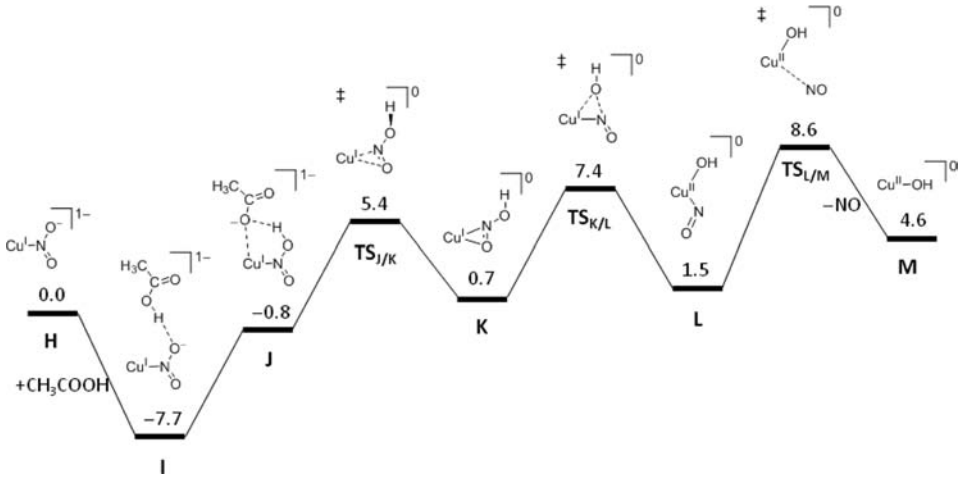

Figure 7. M06/6-31G* free-energy profile for nitrite reduction of **2**.

Computational Results. Computational methods were employed to gain additional information about the detailed reaction mechanisms of nitrite reduction reactions of complexes **1** and **2**. To economize on computing resources, the molecular structures of **1** and **2** were simplified by eliminating three methyl groups distant from the $CuNO_2$ moiety because they are expected to have minor influences on the reactivity. The reaction pathways and the corresponding free-energy changes derived from density functional theory (DFT) M06/6-31G* calculations are summarized in Figures 6 and 7, and the optimized structures for the relevant transition states and intermediates are shown in Figures 8 and 9.

The first step in the reaction of complex **1** (Figures 6 and 8) involves its association with acetic acid to form the H-bonded complex. Two H-bonded conformations, **B** and **B′**, were found to be energy minima (Figure 10). While the two conformations are nearly isoenergetic (**B** is only 0.3 kcal mol^{-1} higher in energy than **B′**), they display very different behaviors in the subsequent proton-transfer step. While proton transfer from acetic acid to NO_2^- in both conformations is barrierless, the energy change occurring is considerably lower for **B** than it is for **B′** (5.8 vs 19.7 kcal mol^{-1}; Figure 10). In conformation **B**, acetic acid is located in close proximity to copper and, therefore, during proton transfer the negative charge accumulated on the conjugate base of the acid can be stabilized by a $CH_3COO^-\cdots Cu^I$ interaction. This stabilizing interaction is reflected in a significant decrease of the $CH_3COO^-\cdots Cu^I$ distance from 3.018 to 2.172 Å in the course of proton transfer (Figure 10). In contrast, this stabilizing interaction is not available in the reaction of conformation **B′** because acetic acid is separated from copper by intervening NO_2^-.

The computational results suggest that the first protonation of NO_2^- is taking place via the H-bonded conformation **B** rather than **B′**, and it results in the formation of the protonated

dx.doi.org/10.1021/ic300932a | Inorg. Chem. 2012, 51, 9297−9308

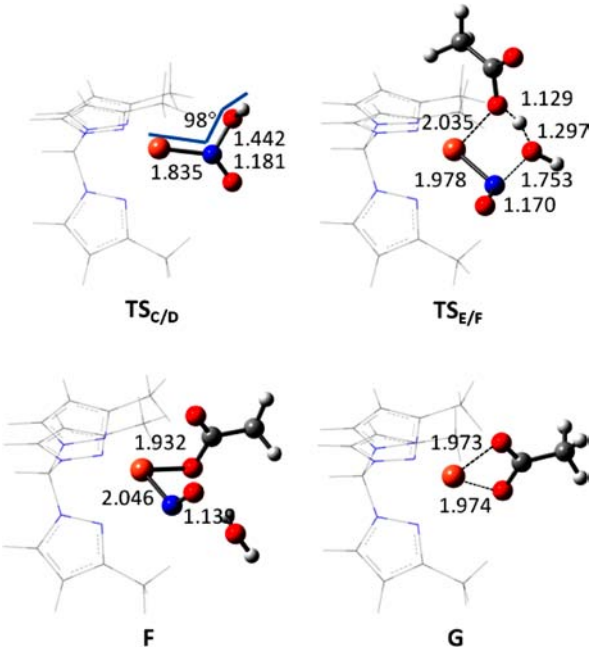

Figure 8. M06/6-31G*-optimized geometries of the transition states and selected intermediates in the course of nitrite reduction of **1**. For clarity, the ligand moieties are represented by wireframes.

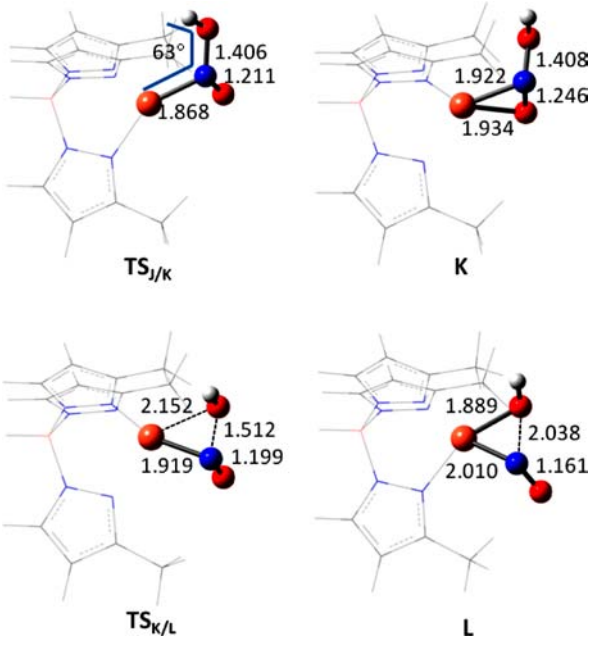

Figure 9. M06/6-31G*-optimized geometries of the transition states and selected intermediates in the course of nitrite reduction of **2**. For clarity, the ligand moieties are represented by wireframes.

structure **C** in which the Cu−NO_2H moiety exists in a syn conformation defined by the H−O−N−Cu relation (Figure 6). To facilitate the second protonation step, a syn−anti transformation is formed through O−H rotation around the N−O bond (**C** → **TS**$_{C/D}$ → **D**). The activation and reaction free-energy changes for this transformation are +7.2 and −5.8 kcal mol^{-1}, respectively. Once the anti conformation **D** is formed, the second acetic acid can approach and bind in a manner that is similar to formation of the H-bonded conformation in the first association step. However, the second

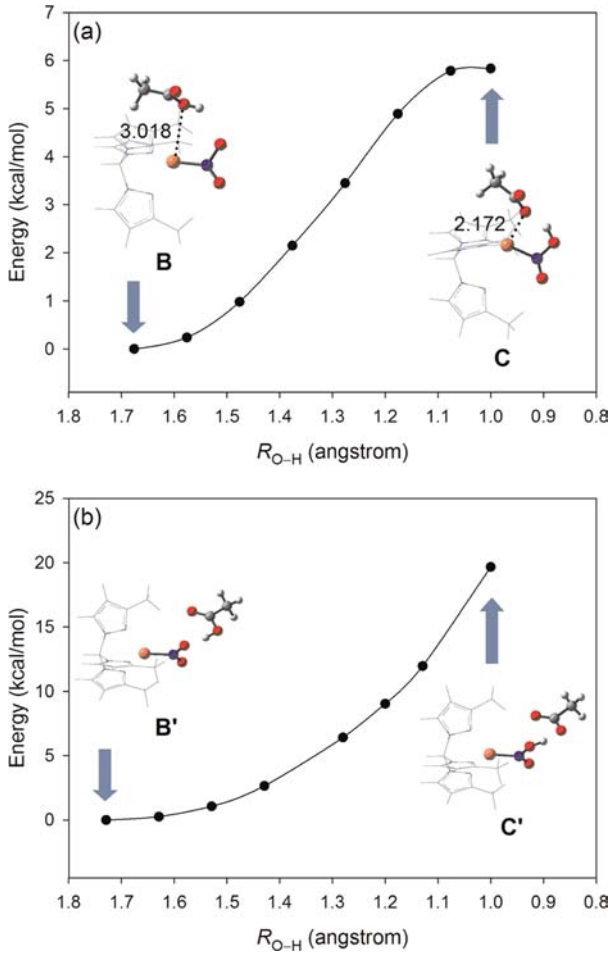

Figure 10. Relaxed potential energy surface scan of proton transfer from acetic acid to NO_2^- for the complex of **1** and acid in H-bonded conformations (a) **B** and (b) **B′**.

association step is thermodynamically less favorable, with an association free energy of 3.1 kcal mol^{-1} (**D** → **E**). Subsequently, the H-bonded complex **E** undergoes the second proton-transfer reaction, leading to cleavage of the N−O bond and the release of a water molecule (**E** → **TS**$_{E/F}$ → **F**). This step is found to be rate-determining with an activation free energy of 18.6 kcal mol^{-1} and a reaction free energy of −6.1 kcal mol^{-1}. The stabilizing interaction between acetate and the copper atom once again plays a role in the second protonation step, as evidenced by a decrease of the O(acetate)···Cu distance from 3.185 Å in **E** to 2.035 Å in **TS**$_{E/F}$ to 1.932 Å in **F** (Figure 8).

The results of wave-function stability tests indicate that the most stable electronic states for **TS**$_{E/F}$ and **F** are singlet biradical rather than closed-shell singlet or triplet. Analysis of the natural population data reveals that the two spins are mainly distributed on copper (the spin densities are 0.4708 in **TS**$_{E/F}$ and 0.5843 in **F**) and NO (the spin densities are −0.5868 in **TS**$_{E/F}$ and −0.7418 in **F**). These results suggest that the second protonation step is a proton-coupled electron-transfer process in which the proton transfer from acetic acid to NO_2H simultaneously triggers an electron transfer from Cu^I to NO_2H. Therefore, the electronic state of **F** is better characterized as Cu^{II}−$NO^{\bullet}$ rather than Cu^I−NO^+. The final step involving liberation of NO (**F** → **G**) has a transition state that is located on the electronic potential energy surface only 0.3 kcal mol^{-1}

dx.doi.org/10.1021/ic300932a | Inorg. Chem. 2012, 51, 9297−9308

above **F** (further correction for the Gibbs free energy would make it lower than **F**). As a consequence, NO release from **F** should be a barrierless process with a free-energy change of −6.1 kcal mol^{-1}. These results indicate that **F** is not a stable intermediate on the free-energy surface and, thus, NO and H_2O dissociate rapidly following (or in concert with) the second protonation process (i.e., the reaction proceeds through **E** → $\mathbf{TS_{E/F}}$ → **G**).

The first two steps in the reaction of complex **2** (Figures 7 and 9) involve the association of **2** with acetic acid and subsequent protonation of nitrite. As is the case with complex **1**, two H-bonded conformations, **I** and **I′**, are found in the pathway for **2** (Figure 11). The free-energy difference between

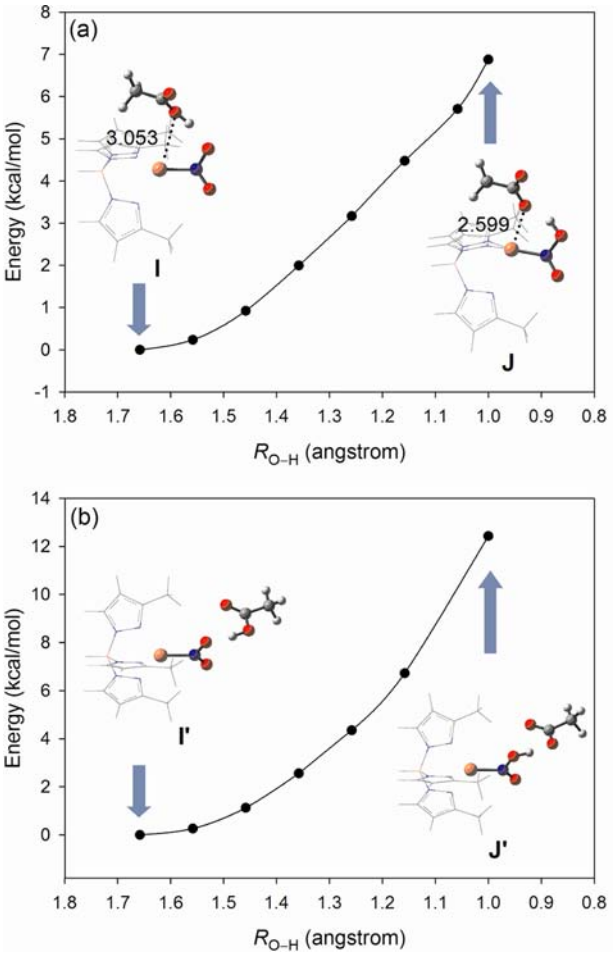

Figure 11. Relaxed potential energy surface scan of proton transfer from acetic acid to NO_2^- for the complex of **2** and acid in H-bonded conformations (a) **I** and (b) **I′**.

I and **I′** is only 0.6 kcal mol^{-1}, with the former being less stable. However, proton transfer from acetic acid to nitrite is calculated to be endergonic by 6.9 kcal mol^{-1} in **I**, more favorable than the endergonicity of 12.4 kcal mol^{-1} in **I′**, due to the $CH_3COO^-\cdots Cu^I$-stabilizing interaction.

Interestingly, the following steps in the reaction of complex **2** were found to be distinct from those of complex **1**. Rotation of O−H around the N−O bond in the *syn*-Cu^I−NO_2H moiety does not result in formation of the anti conformation of Cu^I−NO_2H. Instead, in the course of rotation, the bonding mode between Cu and NO_2H gradually changes and eventually reaches a novel intermediate state with side-on NO coordination (**J** → $\mathbf{TS_{J/K}}$ → **K**). The side-on η^2-N,O-bonding structure, **K**, lies only 1.5 kcal mol^{-1} above the η^1-N-bonding structure, **J**, and the activation free energy for **J** → **K** transformation is only 6.2 kcal mol^{-1}. The side-on bound NO_2H moiety in the intermediate **K** then cleaves to form OH and NO, which then individually coordinate to the copper atom to form intermediate **L**. It should be noted that a hydroxonitrosyl intermediate of this type has been observed in the previous computational studies on Cu-NIRs.[51,52] The results of relative DFT calculations on the Cu^INO system also show an side-on-bound intermediate owing to steric interactions with amino acid residues.[53]

The activation and reaction free-energy changes for **K** → **L** were estimated to be 6.7 and 0.8 kcal mol^{-1}, respectively. Intermediate **L** was found to be a singlet biradical with a spin density of 0.5095 on copper and a spin density of −0.6955 on NO, which means that an electron has been transferred from Cu^I to NO at this stage. To locate the transition state for the final step of the process, involving NO release from the intermediate **L**, a relaxed potential energy surface scan was performed by stretching along the Cu···NO axis. The computational results indicate that the total electronic energy monotonically increases with the Cu···NO distance (Table S3 in the Supporting Information). In other words, the release of NO is an endergonic process and it does not have an energetic barrier. However, as NO leaves, the entropic contribution becomes larger, which, in turn, creates a transition state on the free-energy surface at a Cu···NO distance of ca. 3.1 Å (Table S3 in the Supporting Information). The activation and reaction free energies for the NO release step, **L** → $\mathbf{TS_{L/M}}$ → **M**, were estimated to be 7.1 and 3.1 kcal mol^{-1}, respectively.

In summary, the reaction of complex **1** with acetic acid proceeds through two protonation steps followed by the immediate release of H_2O and NO, and the second protonation step is rate-determining with an activation energy of 18.6 kcal mol^{-1}. Importantly, the DFT results provide a theoretical basis for the experimentally observed curved-line plot of k_{obs} versus $[H^+]$ and the deuterium KIE in the reaction of **1**. On the other hand, the reaction of complex **2** with acetic acid requires only the first protonation step to rupture the N−O bond of nitrite and form a hydroxonitrosyl intermediate. This conclusion explains why the rate of nitrite reduction involving complex **2** is first-order in H^+. Furthermore, the protonation of complex **2** is not rate-determining because other steps in the mechanistic pathway have comparable activation energies. This fact could explain why a deuterium KIE was not observed in the reaction of complex **2**. Finally, the calculated energy barrier for the reaction of **2** (6.2−7.1 kcal mol^{-1}) is considerably lower than that of **1** (18.6 kcal mol^{-1}), an observation that is consistent with the finding that the former complex displays higher reactivity.

Above we described the interesting crystal structure of **3** in which a water molecule acts as hydrogen-bond donor to a nitrite oxygen atom. In addition, evidence exists to support the proposal that several water molecules are present in the active sites of Cu-NIRs.[16] Consequently, it is interesting and important to know how hydrogen bonding affects the catalytic reactivity of these enzymes. The results of our preliminary calculations show that when H_2O is H-bonded to oxygen atoms of nitrite in complexes **1** and **2**, the first protonation step in the overall process leading to NO production is impeded. Specifically, the energy of the protonation step increases from 5.8 to 9.1 kcal mol^{-1} and from 6.9 to 11.5 kcal mol^{-1} for the

dx.doi.org/10.1021/ic300932a | *Inorg. Chem.* 2012, 51, 9297−9308

Scheme 3. Proposed Mechanism for Nitrite Reduction of 1

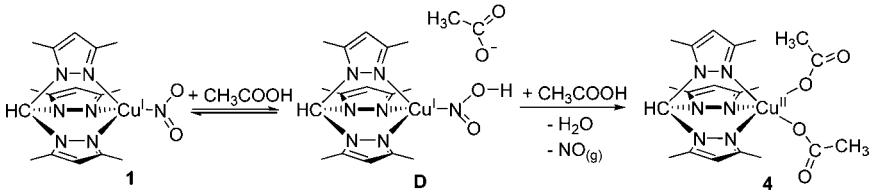

Scheme 4. Proposed Mechanism for Nitrite Reduction of 2

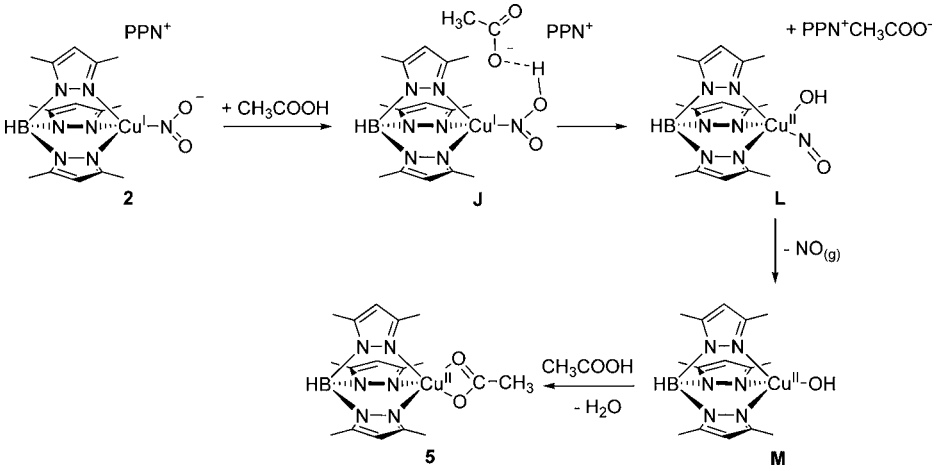

reactions of **1** and **2**, respectively. This result leads to a tentative conclusion that the nitrite reduction reactivity is reduced when the oxygen atom of nitrite is H-bonded to a water molecule. Further computational studies that consider the hydrogen-bonding effects on other steps of the reaction mechanism, the influence of different hydrogen-bonding conformations, and the number of water molecules are needed to fully understand this issue.

Nitrite Reduction Mechanisms. On the basis of information found in the literature and the results of our computational calculations,[26,28] we suggest that the mechanism concisely presented in Scheme 3 is operable in the nitrite reduction process of the neutral ligand containing complex **1**. The existence of the protonated intermediate **D** in this process is supported by studies by Kujime et al., in which a nitrous acid intermediate ($CuNO_2H$) was detected in a stopped-flow experiment involving the rapid mixing of [(^{i}Pr-TACN)Cu(NO_2)] with trifluoroacetic acid at low temperature.[28,29] Intermediate **D**, subsequently, reacts with acid followed by the release of NO to give the copper(II) acetate product **4**. This mechanism was proposed earlier by Fujii and co-workers based on the results of kinetic measurements.[28] In the current effort, we isolated the final product of this process in the form of complexes **4** and **6** containing carboxylate anions bound to copper.

The nitrite reduction mechanism for the reaction of complex **2** with acetic acid is displayed in Scheme 4. Importantly, titration experiments of **2** with acetic acid, consuming 1 equiv of acetic acid, support this proposed mechanism. The protonated intermediate **J** in this pathway is similar to the nitrous acid intermediate ($CuNO_2H$) **D**. The novel complex **3**, containing an anionic copper(I) nitro unit with an H-bonded water molecule, isolated in this effort represents the first example of an analogue of the nitrous acid intermediate ($CuNO_2H$). Recently, Solomon et al. suggested that the nitrite reduction process is best thought about as proton transfer triggering an electron-transfer reaction.[21] Therefore, the formation of intermediate **J** might trigger rearrangement and electron transfer to form intermediate **L**, which then releases NO to give intermediate **M**. Several $Cu^{II}OH$ complexes stabilized by tris(pyrazolyl)borate ligands have been described, and these serve as precedents for intermediate **M**.[54−56] Finally, protonation of **M** leads to the elimination water and acetate anion binding to generate **5**.

CONCLUSION

In summary, copper(I) nitrite complexes **1** and **2**, containing the respective neutral $HC(3,5\text{-}Me_2Pz)_3$ or anionic $[HB(3,5\text{-}Me_2Pz)_3]^-$ tripodal scorpionate ligands, have been prepared as models of the active site of dissimilatory Cu-NIRs. X-ray crystal structural analysis of **2** reveals that the geometry of the copper center is a distorted tetrahedral and nitrite is N-coordinated to copper. The results of a mechanism study show that in reactions of these complexes with acetic acid the protonation steps are not rate-determining. The nitrite reduction reactivity of neutral and anionic copper(I) nitro complexes are significantly influenced by the electron density around copper and nitrite. The highly reactive, anionic ligand containing complex **2** forms a new copper(I) nitro complex, **3**, with a cocrystallized water molecule that is H-bonded to an oxygen atom of the copper(I) nitro moiety. Complex **3** represents the first example of a solid-state nitrous acid intermediate ($CuNO_2H$) analogue. The results of DFT calculations show that nitrite reduction reactions of **1** and **2** proceed through different mechanistic pathways.

A survey of the literature shows that most copper(I) nitro bonding mode complexes possessing trinitrogen-donor auxiliary ligands release NO gas upon treatment with acid.[25,26,28] However, no examples exist of copper(I) nitrito complexes with trinitrogen donors as auxiliary ligands undergoing this process.

dx.doi.org/10.1021/ic300932a | Inorg. Chem. 2012, 51, 9297−9308

Only two copper(I) nitrito complexes containing phosphine ligands have been observed to release NO gas under acidic conditions.[30,31] Because phosphine ligands are unsuitable models of the imidazole ligand, the copper(I) nitrito phosphine complexes are not good structural models for Cu-NIRs. On the basis of the results accumulated thus far, we believe that copper(I) nitro complexes containing neutral $HC(3,5\text{-}Me_2Pz)_3$ or anionic $[HB(3,5\text{-}Me_2Pz)_3]^-$ ligands serve as the best synthetic models of the type II copper centers in enzymes that promote nitrite reduction.

EXPERIMENTAL SECTION

All manipulations involving copper(I) complexes were carried out under an atmosphere of purified N_2 in a drybox or using standard Schlenk techniques. Chemical reagents were purchased from Aldrich Chemical Co. Ltd., Lancaster Chemicals Ltd., or Fluka Ltd. All of the reagents were used without further purification, apart from all solvents, which were dried over Na (Et_2O and THF) or CaH_2 (CH_2Cl_2, and CH_3CN) and then thoroughly degassed before use. The copper(I) complexes $[Cu(HC(3,5\text{-}Me_2Pz)_3)(NCMe)](BF_4)$[41] and $[HB(3,5\text{-}Me_2Pz)_3Cu]_2$[42] were prepared as described in the literature. IR spectra were recorded on a Varian FT-IR 640 spectrometer. UV−vis spectra were recorded on an Agilent 8453 spectrophotometer. ^1H, ^{13}C, and ^{31}P NMR spectra were acquired on a Varian Gemini-200 proton/carbon FT-NMR spectrometer or a Varian Gemini-500 proton/carbon FT-NMR spectrometer. ESI-MS spectra were collected on a Waters ZQ 4000 mass spectrometer. Elemental analyses were performed on a Heraeus CHN-OS rapid elemental analyzer. Cyclic voltammetry was measured at a scan rate of 100 mV s^{-1} at around 10^{-4} M CH_2Cl_2 solutions using 0.1 M $[n\text{-}Bu_4N](PF_6)$ as the supporting electrolyte and referenced to $Fc^{+/0}$. GC-TCD experiments were performed using a Varian CP- 3800 gas chromatograph, a Porpak Q column (6 ft, 20 mL min^{-1} flow rate, 30 °C, nitrogen carrier gas), and a TCD.

$[Cu(HC(3,5\text{-}MePz)_3)(NO_2)]$ (1). A solution of $[Cu(HC(3,5\text{-}Me_2Pz)_3)(NCMe)](BF_4)$ (0.205 g, 0.420 mmol) in 10 mL of methanol was added to a solution of sodium nitrite (0.144 g, 2.095 mmol) in 5 mL of methanol. A yellow solid precipitate formed immediately. The resulting precipitate was isolated by filtration, washed with methanol (5 mL), and dried under vacuum at room temperature to give a yellow product (0.12 g, 70%). Anal. Calcd for $C_{16}H_{22}O_2N_7Cu$: C, 47.11; H, 5.44; N, 24.03. Found: C, 47.27; H, 5.51; N, 23.95. ^1H NMR (acetone-d^6): δ 7.85 (s, 1H, *HC*(3,5-$Me_2Pz)_3$), 6.12 (s, 3H, 4-*H*Pz), 2.54 (s, 9H, *Me*$_2$Pz), 2.38 (s, 9H, *Me*$_2$Pz). IR (KBr, cm^{-1}): $\nu(NO_2)$ 3141, 2986, 2958, 2923, 1565, 1467, 1413, 1389, 1312 (1289, $^{15}NO_2^-$), 1285 (1262, $^{15}NO_2^-$), 1240, 1155, 1099, 1039, 980, 899, 849, 824 (814, $^{15}NO_2^-$), 801, 705, 698, 631. ESI-MS(+): m/z 361.29 ($[Cu(HC(3,5\text{-}MePz)_3)]^+$).

$[(Ph_3P)_2N][Cu(HB(3,5\text{-}MePz)_3)(NO_2)]$ (2). In a glovebox, a solution of $[(Ph_3P)_2N](NO_2)$ (0.162 g, 0.277 mmol) in 20 mL of THF was added to a solution of $[HB(3,5\text{-}Me_2Pz)_3Cu]_2$ (0.1 g, 0.138 mmol) in 5 mL of THF followed by stirring for 30 min. The solution was kept at −20 °C for 3 days to yield yellow crystals (0.13 g, 0.138 mmol, 50%). Anal. Calcd for $C_{51}H_{52}BCuN_8O_2P_2$: C, 64.80; H, 5.54; N, 11.85. Found: C, 64.77; H, 5.81; N, 11.83. ^1H NMR (acetone-d^6): δ 7.58−7.78 (m), 5.76 (s, 3H, 4-*H*(Pz)), 2.41 (s, 9H, C*Me*), 2.30 (s, 9H, C*Me*). IR (KBr, cm^{-1}): 2922, 2470, 1542, 1438, 1302 (1284, $^{15}NO_2^-$), 1267 (1265, $^{15}NO_2^-$), 1186, 1115, 754 (746, $^{15}NO_2^-$), 723, 694. ESI-MS(−): m/z 406.26 ($[Cu(HB(3,5\text{-}Me_2Pz)_3)(NO_2)]^-$).

$[(Ph_3P)_2N][Cu(HB(3,5\text{-}MePz)_3)(NO_2)]\cdot H_2O$ (3). In a glovebox, **2** (0.1 g, 0.10 6 mmol) was dissolved in 2 mL of degassed wet THF and kept at −20 °C for 7 days to yield yellow crystals (0.03 g, 30%). Anal. Calcd for $C_{51}H_{54}O_3N_8BCuP_2$: C, 63.59; H, 5.65; N, 11.63. Found: C, 63.37; H, 5.51; N, 11.68.

Kinetics. Kinetic studies of nitrite reduction of **1** or **2** in CH_2Cl_2 were carried out by monitoring decreases in the intensities of the 262 and 336 nm absorption bands, respectively. The absorbance was detected by using an Agilent 8453 spectrophotometer equipped with an UNISOKU USP-203A cryostat or a custom-designed fiber-optic immersion quartz probe of 1 cm path length (Hellma) and fitted to a Schlenk flask containing 50 mL of a CH_2Cl_2 solution of **1** or **2** (both 0.25 mM) under a N_2 atmosphere. The reaction was started with the addition of 360 μL of acetic acid, which was degassed with N_2 before use.

Measurement of NO Generation. A solution of **2** (56.7 mg, 0.059 mmol) in CH_2Cl_2 (0.9 mL) was prepared in a small vial capped with a rubber septum. A solution of trifluoroacetic acid (30 μL) in CH_2Cl_2 (0.1 mL) was then introduced with a syringe at room temperature. The solution changed immediately from colorless to blue. Analysis of the headspace gas by a TCD indicated that NO had been generated (83.3 ± 2.3 for **2**). The NO generation data are obtained by using three different experiments (see Table 3 and Figure S10 in the Supporting Information). NO concentrations were determined by using a calibration curve correlating responses to known concentrations of NO gas mixed with N_2 (120, 100, 80, 60, and 40 ppm of NO in N_2); molar quantities were calculated using the ideal gas equation.

X-ray Crystal Structure Determinations. All single-crystal X-ray diffraction data were accumulated using a Bruker Nonius Kappa CCD diffractometer using Mo Kα radiation (λ = 0.71073 Å). The data collection was executed using the *SMART* program.[57] Cell refinement and data reduction were made with the *SAINT* program.[58] The structure was determined using the *SHELXTL/PC* program[59] and refined using full-matrix least squares. All non-hydrogen atoms were refined anisotropically, whereas hydrogen atoms were placed at calculated positions and included in the final stage of refinement with fixed parameters. The disordered THF solvent molecules in complex **2** were removed from the diffraction data using the *SQUEEZE* program. Further details are given in Table S4 in the Supporting Information.

Computational Method. All DFT calculations were carried out using the *Gaussian 09* program.[60] The hybrid meta functional, M06, combined with 6-31G* (5D, 7F) basis functions was used throughout in this work. The M06 functional was chosen because it has been shown to have good performance for many areas of chemical problems, including main-group thermochemistry, kinetics, noncovalent interactions, and, in particular, transition-metal thermochemistry.[61,62] An ultrafine grid, specified by the "integral(grid=ultrafinegrid)" keyword, was used for numerical integrations. Vibrational frequency analysis was performed for each optimized structure to identify whether it is an equilibrium structure or a transition state. The thermal correction to Gibbs free energy was made under the conditions of 298.15 K and 1 atm. The "stable=opt" keyword was used to test the wave-function stability as well as to obtain a stable broken-symmetry solution (i.e., singlet biradical) if instability exists. Once the broken-symmetry wave function was found, the geometry was reoptimized in this electronic state. The spin densities were evaluated using the natural population analysis method.

ASSOCIATED CONTENT

Supporting Information

Additional figures (Figure S1−S14) and tables (Table S1−S4) and crystallographic data in CIF format for the structure determinations of **2**, **3**, and **6**. This material is available free of charge via the Internet at http://pubs.acs.org.

AUTHOR INFORMATION

Corresponding Author

*E-mail: sodiohsu@kmu.edu.tw (S.C.N.H.), hychen@kmu.edu.tw (H.-Y.C.).

Notes

The authors declare no competing financial interest.

ACKNOWLEDGMENTS

Financial support for this study by a grant from the National Science Council (Taiwan) is highly appreciated (NSC Grant 100-2113-M-037-006-MY2). We thank Ting-Shen Kuo, Na-

tional Taiwan Normal University, and Yi-Hung Liu, National Taiwan University, for X-ray structural determinations, Professor Way-Zen Lee, National Taiwan Normal University, for his assistance on the low-temperature UV−vis monitoring experiments, and the National Center for High-Performance Computing for providing computational resources.

REFERENCES

(1) Wasser, I. M.; de Vries, S.; Moenne-Loccoz, P.; Schroder, I.; Karlin, K. D. *Chem. Rev.* **2002**, *102*, 1201.
(2) Suzuki, S.; Kataoka, K.; Yamaguchi, K. *Acc. Chem. Res.* **2000**, *33*, 728.
(3) Averill, B. A. *Chem. Rev.* **1996**, *96*, 2951.
(4) Godden, J. W.; Turley, S.; Teller, D. C.; Adman, E. T.; Liu, M. Y.; Payne, W. J.; LeGall, J. *Science* **1991**, *253*, 438.
(5) Kukimoto, M.; Nishiyama, M.; Murphy, M. E. P.; Turley, S.; Adman, E. T.; Horinouchi, S.; Beppu, T. *Biochemistry* **1994**, *33*, 5246.
(6) Howes, B. D.; Abraham, Z. H. L.; Lowe, D. J.; Bruser, T.; Eady, R. R.; Smith, B. E. *Biochemistry* **1994**, *33*, 3171.
(7) Suzuki, S.; Kohzuma, T.; Deligeer; Yamaguchi, K.; Nakamura, N. *J. Am. Chem. Soc.* **1994**, *116*, 11145.
(8) Suzuki, S.; Deligeer; Yamaguchi, K.; Kataoka, K.; Kobayashi, K.; Tagawa, S.; Kohzuma, T.; Shidara, S.; Iwasaki, H. *J. Biol. Inorg. Chem.* **1997**, *2*, 265.
(9) Farver, O.; Eady, R. R.; Abraham, Z. H. L.; Pecht, I. *FEBS Lett.* **1998**, *436*, 239.
(10) Merkle, A. C.; Lehnert, N. *Dalton Trans.* **2012**, *41*, 3355.
(11) Hulse, C. L.; Averill, B. A. *J. Am. Chem. Soc.* **1989**, *111*, 2322.
(12) Jackson, M. A.; Tiedje, J. M.; Averill, B. A. *FEBS Lett.* **1991**, *291*, 41.
(13) Strange, R. W.; Murphy, L. M.; Dodd, F. E.; Abraham, Z. H. L.; Eady, R. R. *J. Mol. Biol.* **1999**, *287*, 1001.
(14) Ye, R. W.; Toro-Suarez, I.; Tiedje, J. M.; Averill, B. A. *J. Biol. Chem.* **1991**, *266*, 12848.
(15) Boulanger, M. J.; Kukimoto, M.; Nishiyama, M.; Horinouchi, S.; Murphy, M. E. P. *J. Biol. Chem.* **2000**, *275*, 23957.
(16) Murphy, M. E. P.; Turley, S.; Adman, E. T. *J. Biol. Chem.* **1997**, *272*, 28455.
(17) Kataoka, K.; Furusawa, H.; Takagi, K.; Yamaguchi, K.; Suzuki, S. *J. Biochem.* **2000**, *127*, 345.
(18) Zhao, Y.; Lukoyanov, D. A.; Toropov, Y. V.; Wu, K.; Shapleigh, J. P.; Scholes, C. P. *Biochemistry* **2002**, *41*, 7464.
(19) Antonyuk, S. V.; Strange, R. W.; Sawers, G.; Eady, R. R.; Hasnain, S. S. *Proc. Natl. Acad. Sci. U.S.A.* **2005**, *102*, 12041.
(20) Tocheva, E. I.; Rosell, F. I.; Mauk, A. G.; Murphy, M. E. P. *Science* **2007**, *304*, 867.
(21) Ghosh, S.; Dey, A.; Sun, Y.; Scholes, C. P.; Solomon, E. I. *J. Am. Chem. Soc.* **2009**, *131*, 277.
(22) Nojiri, M.; Koteishi, H.; Nakagami, T.; Kobayashi, K.; Inoue, T.; Yamaguchi, K.; Suzuki, S. *Nature* **2009**, *462*, 117.
(23) Halfen, J. A.; Mahapatra, S.; Olmstead, M. M.; Tolman, W. B. *J. Am. Chem. Soc.* **1994**, *116*, 2173.
(24) Halfen, J. A.; Tolman, W. B. *J. Am. Chem. Soc.* **1994**, *116*, 5475.
(25) Halfen, J. A.; Mahapatra, S.; Wilkinson, E. C.; Gengenbach, A. J.; Young, V. G., Jr.; Que, L., Jr.; Tolman, W. B. *J. Am. Chem. Soc.* **1996**, *118*, 763.
(26) Yokoyama, H.; Yamaguchi, K.; Sugimoto, M.; Suzuki, S. *Eur. J. Inorg. Chem.* **2005**, 1435.
(27) Nairn, A. K.; Archibald, S. J.; Bhalla, R.; Boxwell, C. J.; Whitwood, A. C.; Walton, P. H. *Dalton Trans.* **2006**, 1790.
(28) Kujime, M.; Izumi, C.; Tomura, M.; Hada, M.; Fujii, H. *J. Am. Chem. Soc.* **2008**, *130*, 6088.
(29) Kujime, M.; Fujii, H. *Angew. Chem., Int. Ed.* **2006**, *45*, 1089.
(30) Chuang, W.-J.; Lin, I. J.; Chen, H.-Y.; Chang, Y.-L.; Hsu, S. C. N. *Inorg. Chem.* **2010**, *49*, 5377.
(31) Chen, C.-S.; Yeh, W.-Y. *Chem. Commun.* **2010**, *46*, 3098.
(32) Kalita, A.; Kumar, P.; Deka, R. C.; Mondal, B. *Chem. Commun.* **2012**, *48*, 1251.
(33) Ruggiero, C. E.; Carrier, S. M.; Tolman, W. B. *Angew. Chem.* **1994**, *106*, 917.
(34) Tolman, W. B. *Inorg. Chem.* **1991**, *30*, 4877.
(35) Lehnert, N.; Cornelissen, U.; Neese, F.; Ono, T.; Noguchi, Y.; Okamoto, K.-i.; Fujisawa, K. *Inorg. Chem.* **2007**, *46*, 3916.
(36) Carrier, S. M.; Ruggiero, C. E.; Tolman, W. B. *J. Am. Chem. Soc.* **1992**, *114*, 4407.
(37) Carrier, S. M.; Ruggiero, C. E.; Houser, R. P.; Tolman, W. B. *Inorg. Chem.* **1993**, *32*, 4889.
(38) Schneider, J. L.; Carrier, S. M.; Ruggiero, C. E.; Young, V. G., Jr.; Tolman, W. B. *J. Am. Chem. Soc.* **1998**, *120*, 11408.
(39) Fujisawa, K.; Tateda, A.; Miyashita, Y.; Okamoto, K.; Paulat, F.; Praneeth, V. K. K.; Merkle, A.; Lehnert, N. *J. Am. Chem. Soc.* **2008**, *130*, 1205.
(40) Kumar, M.; Dixon, N. A.; Merkle, A. C.; Zeller, M.; Lehnert, N.; Papish, E. T. *Inorg. Chem.* **2012**, *51*, 7004.
(41) Hsu, S. C. N.; Chen, H. H. Z.; Lin, I.-J.; Liu, J.-J.; Chen, P.-Y. *J. Organomet. Chem.* **2007**, *692*, 3676.
(42) Mealli, C.; Arcus, C. S.; Wilkinson, J. L.; Marks, T. J.; Ibers, J. A. *J. Am. Chem. Soc.* **1976**, *98*, 711.
(43) Fujisawa, K.; Ono, T.; Ishikawa, Y.; Amir, N.; Miyashita, Y.; Okamoto, K.-i.; Lehnert, N. *Inorg. Chem.* **2006**, *45*, 1698.
(44) Jeffrey, G. A. *An Introduction to Hydrogen Bonding*; Oxford University Press: Oxford, U.K., 1997.
(45) Kay, M. I.; Frazer, B. C. *Acta Crystallogr.* **1961**, *B24*, 56.
(46) Fujisawa, K.; Noguchi, Y.; Miyashita, Y.; Okamoto, K.-i.; Lehnert, N. *Inorg. Chem.* **2007**, *46*, 10607.
(47) Basallote, M. G.; Duran, J.; Fernandez-Trujillo, M. J.; Manez, M. A.; Torre, J. R. *J. Chem. Soc., Dalton Trans.* **1998**, 745.
(48) Addison, A. W.; Rao, T. N.; Reedijk, J.; Rijn, J. v.; Verschoor, G. C. *J. Chem. Soc., Dalton Trans.* **1984**, 1349.
(49) Fujisawa, K.; Miyashita, Y.; Yamada, Y.; Okamoto, K. *Bull. Chem. Soc. Jpn.* **2001**, *74*, 1065.
(50) Moubaraki, B.; Murray, K. S.; Tiekink, E. R. T. *Z. Kristallogr., New Cryst. Struct.* **2002**, *217*, 219.
(51) De Marothy, S. A.; Blomberg, M. R. A.; Siegbahn, P. E. M. *J. Comput. Chem.* **2007**, *28*, 528.
(52) Sundararajan, M.; Hillier, I. H.; Burton, N. A. *J. Phys. Chem. B* **2007**, *111*, 5511.
(53) Merkle, A. C.; Lehnert, N. *Inorg. Chem.* **2009**, *48*, 11504.
(54) Fujisawa, K.; Kobayashi, T.; Fujita, K.; Kitajima, N.; Moro-oka, Y.; Miyashita, Y.; Yamada, Y.; Okamoto, K.-i. *Bull. Chem. Soc. Jpn.* **2000**, *73*, 1797.
(55) Kitajima, N.; Koda, T.; Hashimoto, S.; Kitagawa, T.; Morooka, Y. *J. Am. Chem. Soc.* **1991**, *113*, 5664.
(56) Kitajima, N.; Fujisawa, K.; Fujimoto, C.; Morooka, Y.; Hashimoto, S.; Kitagawa, T.; Toriumi, K.; Tatsumi, K.; Nakamura, A. *J. Am. Chem. Soc.* **1992**, *114*, 1277.
(57) Sheldrick, G. M. *SHELXL-97, Program for the Refinement of Crystal Structures*; University of Göttingen: Göttingen, Germany, 1997.
(58) *SAINT Manual*, version 5/6.0; Bruker Analytical X-ray Systems Inc.: Madison, WI, 1997.
(59) *SHELXTL-PC Manual*, version 5.1; Bruker Analytical X-ray Systems Inc.: Madison, WI, 1997.
(60) Frisch, M. J.; Trucks, G. W.; Schlegel, H. B.; Scuseria, G. E.; Robb, M. A.; Cheeseman, J. R.; Montgomery, J. A., Jr.; Vreven, T.; Kudin, K. N.; Burant, J. C.; Millam, J. M.; Iyengar, S. S.; Tomasi, J.; Barone, V.; Mennucci, B.; Cossi, M.; Scalmani, G.; Rega, N.; Petersson, G. A.; Nakatsuji, H.; Hada, M.; Ehara, M.; Toyota, K.; Fukuda, R.; Hasegawa, J.; Ishida, M.; Nakajima, T.; Honda, Y.; Kitao, O.; Nakai, H.; Klene, M.; Li, X.; Knox, J. E.; Hratchian, H. P.; Cross, J. B.; Bakken, V.; Adamo, C.; Jaramillo, J.; Gomperts, R.; Stratmann, R. E.; Yazyev, O.; Austin, A. J.; Cammi, R.; Pomelli, C.; Ochterski, J. W.; Ayala, P. Y.; Morokuma, K.; Voth, G. A.; Salvador, P.; Dannenberg, J. J.; Zakrzewski, V. G.; Dapprich, S.; Daniels, A. D.; Strain, M. C.; Farkas, O.; Malick, D. K.; Rabuck, A. D.; Raghavachari, K.; Foresman, J. B.; Ortiz, J. V.; Cui, Q.; Baboul, A. G.; Clifford, S.; Cioslowski, J.; Stefanov, B. B.; Liu, G.; Liashenko, A.; Piskorz, P.; Komaromi, I.; Martin, R. L.; Fox, D. J.; Keith, T.; Al-Laham, M. A.; Peng, C. Y.;

Nanayakkara, A.; Challacombe, M.; Gill, P. M. G.; Johnson, B.; Chen, W.; Wong, M. W.; Gonzalez, C.; Pople, J. A. *Gaussian 09*, revision A.02; Gaussian, Inc.: Wallingford, CT, 2009.
(61) Zhao, Y.; Truhlar, D. *Theor. Chem. Acc.* **2008**, *120*, 215.
(62) Zhao, Y.; Truhlar, D. G. *Acc. Chem. Res.* **2008**, *41*, 157.